KLOE note n.152
October 1995

Tests on Full Size Modules of the KLOE Electromagnetic Calorimeter.

M. Antonelli[b], G. Barbiellini[g], M. Barone[b], H. Beker[d], S. Bertolucci[b], C. Bini[d], C. Bloise[b], R. Caloi[d], P. Campana[b], F. Cervelli[c], M. Cordelli[b], G. De Zorzi[d], G. Di Cosimo[d], A. Di Domenico[d], F. Donno[b], O. Erriquez[a], A. Farilla[a], A. Ferrari[c], P. Franzini[d], P. Gauzzi[d], E. Gero[b], S. Giovannella[b], M. Incagli[c], L. Keeble[b], W. Kim[f], G. Lanfranchi[b], J. Lee-Franzini[b,f], A. Martini[b], A. Martinis[g], S. Miscetti[b], F. Murtas[b], A. Passeri[e], F. Scuri[g], E. Spiriti[e], L. Tortora[e], G. Venanzoni[c], S.Wölfle[b], J.Zhang[b]

[a] *Dipartimento di Fisica dell'Università e Sezione INFN Bari, Italy*
[b] *Laboratori Nazionali di Frascati dell'INFN Frascati, Italy*
[c] *Dipartimento di Fisica dell'Università e Sezione INFN Pisa, Italy*
[d] *Dipartimento di Fisica dell'Università e Sezione INFN Roma I, Italy*
[e] *Istituto Superiore di Sanità and Sezione INFN ISS Roma, Italy*
[f] *Physics Department State University of New York at Stony Brook, USA*
[g] *Dipartimento di Fisica dell'Università e Sezione INFN Trieste/Udine, Italy*

ABSTRACT

The KLOE electromagnetic calorimeter is a very fine sampling lead - scintillating fiber calorimeter. The first full size barrel module, equipped with 11.5 cm Kuraray SCSF-81 followed by 11.5 cm Pol.Hi.Tech. 0046 fibers and read out with Hamamatsu R5946/01 mesh photomultipliers, was exposed to a test beam at PSI (near Zurich) where an energy resolution of $\sigma_E/E \sim 5\%/\sqrt{E\ (\mathrm{GeV})}$ and a time resolution of $\sigma_T \sim 72\ \mathrm{ps}/\sqrt{E\ (\mathrm{GeV})}$ were found. Since the test beam it has been continuously monitored with cosmic rays in a test set up with triggering and tracking devices, collecting data with cosmic rays for continuous monitoring. The final version of the calorimeter will be equipped with photomultipliers with higher quantum efficiencies, and the second half of the calorimeter will be equipped with high quality Pol.Hi.Tech fibers as well, thus an energy resolution of $\sigma_E/E \sim 4.7\%/\sqrt{E\ (\mathrm{GeV})}$ and a time resolution of $\sigma_T \sim 50\mathrm{ps}/\sqrt{E\ (\mathrm{GeV})}$ are expected to be the final detector parameters.

1. Introduction

The KLOE experiment[1] at the Frascati Φ-Factory DAΦNE has been designed mainly for the study of the CP violation in the decays of the neutral Kaons. The electromagnetic calorimeter should detect the $20 - 280\ MeV$ photons coming from the π^0 produced in the $K_{L,S} \rightarrow \pi^0\pi^0$ decays and measure the $K_{L,S}$ decay vertex. Full detection efficiency down to $20\ MeV$, hermeticity, good energy and time resolutions are the requirements for such a calorimeter.

A lead-scintillating fibers sampling calorimeter has been chosen and it is now under construction. Results on a smaller size prototype[2] had shown that the required energy and time resolutions in the energy range of the experiment could be obtained.

In this paper results concerning the performance of the first full size module of the KLOE electromagnetic calorimeter are presented. In Section 2 the calorimeter is described in some detail, while Sections 3 and 4 present results concerning a test-beam done at PSI (Sect. 3) and the continuous monitoring of the performance obtained by using cosmic rays (Sect. 4).

2. Calorimeter description

The KLOE electromagnetic calorimeter is a very fine sampling lead-scintillating fiber calorimeter. The central part, barrel, approximating a cylindrical shell of 4 m inner diameter, 4.3 m active length and 23 cm thickness (about 15 radiation lengths), consists of 24 modules with trapezoidal cross section and with the fibers running parallel to the DAΦNE circulating beams. Two end-caps close the calorimeter providing hermetical coverage. Each of them consists of 32 "C" shaped 23 cm thick modules with fibers running perpendicular to the circulating beams and bent at 90^o in such a way to make the read-out possible. In Fig. 1 a quarter of the KLOE detector is shown.

Each module is built by glueing 1 mm diameter scintillating fibers between thin grooved lead plates, obtained by passing 0.5 mm thick lead foils through rollers of proper shape. This results in a structure which has a fiber:lead:glue volume ratio of 48:42:10 and a sampling fraction of $\sim 13\%$. Kuraray SCSF-81 and Pol.Hi.Tech. 0046 fibers are used[3] (both emitting light in the "blue" region).

The modules are read-out on the two sides through plexiglas pipes which provide light mixing and terminate with Winston concentrators optically coupled to fine mesh PM's (Hamamatsu R5946/01) that can be used in a magnetic field up to the values expected in KLOE[4] . The PM's high voltages are adjusted such as the same gain of $\sim 5 \times 10^6$ on all channels is achieved. Every barrel module is read-out through 60 channels per side, the read-out granularity being in average 4.5×4.5 cm^2. Fig. 2 shows the front view of one barrel module. There are five planes parallel to the y direction and 12 columns parallel to the x direction. The z coordinate is obtained by the time difference between the two sides. The overall number of read-out channels is about 5000.

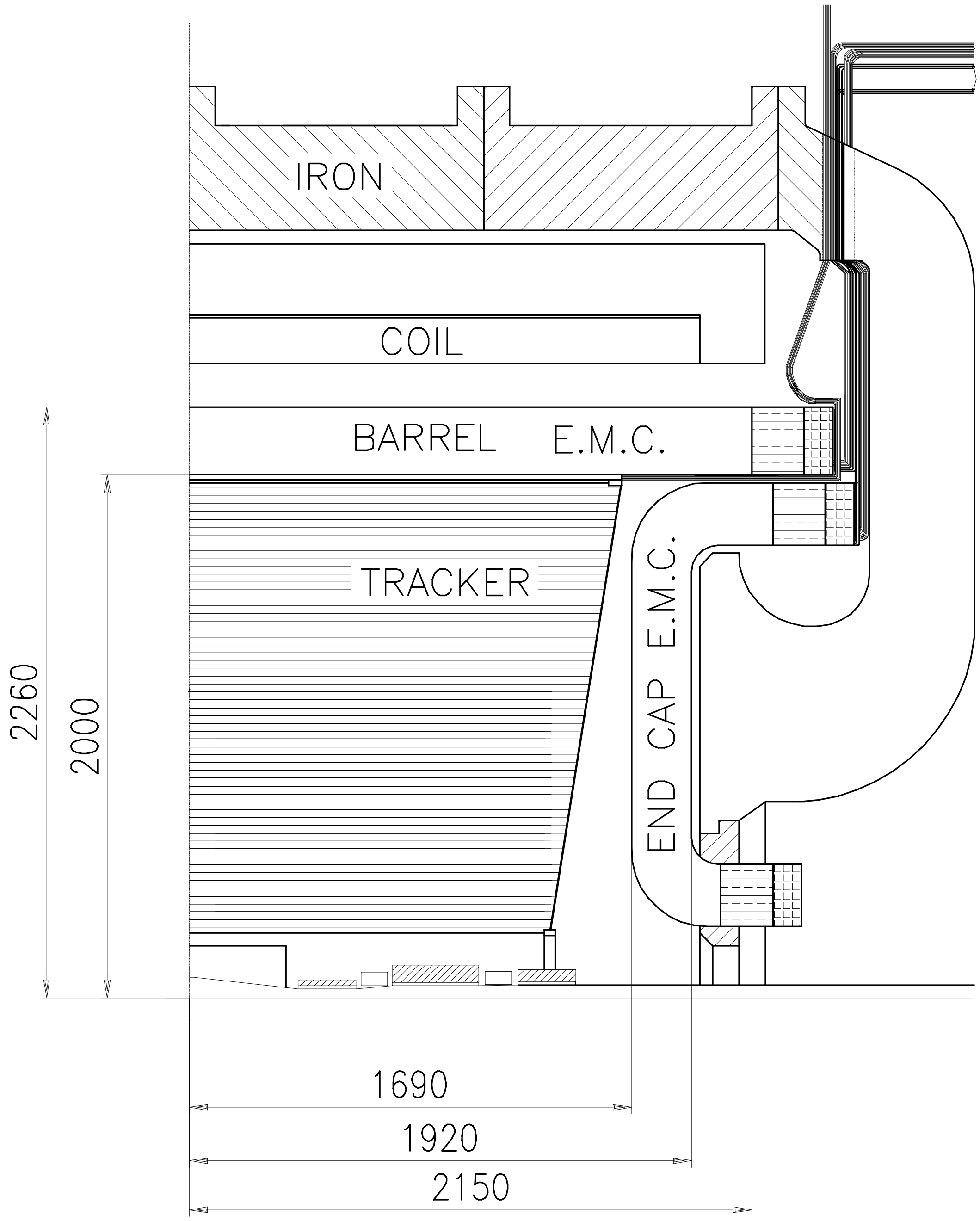

Fig. 1 Side view of a quarter of the KLOE detector. The barrel and the end-caps are shown.

The first full size barrel module has been built and has been equipped with the final light pipes and proto-versions of the final PM's and with KLOE custom designed front-end electronics. Commercial ADC and TDC CAMAC (25 ps/channel) are used for the read-out that is based on a CPU FIC 8246 from CES.

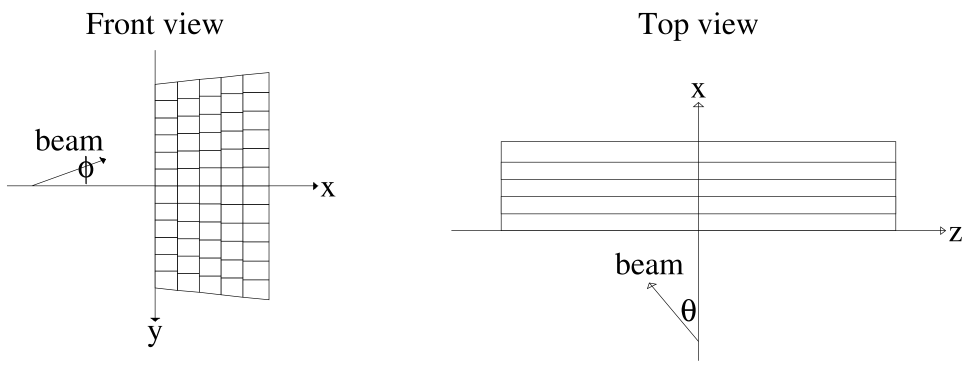

Fig. 2 Sketch of the experimental set-up.The beam line is parallel to the x-axis. In some data taking the module was moved in such a way to scan different θ-φ angles.

3. Test beam results

The "Module Zero" for the KLOE electromagnetic calorimeter was taken to the Paul Scherrer Institut PSI in July 1994 to be tested with electron, muon and pion beams in a momentum range 100 – 450 MeV/c.

3.1 Experimental Setup

The experimental set-up is sketched in fig. 2. The ccordinate system and the angles are defined in the figure. The coincidence of three scintillator counters was acting as the trigger signal, two of them formed a cross right in front of the calorimeter, thus defining a beam spot of 1.0×1.0 cm^2. The third one was located at a distance of 3.5 m in upstream direction to enable time of flight measurements necessary for particle identification. One of the two crossed scintillators was used as start signal for the TDCs, the time difference between the two was used as estimate of the start jitter.

The beam was a mixture of e^-, μ^- and π^- in a proportion depending on the energy. They could be distinguished event by event by their time of flight between the trigger counters.

In the following, the results using electrons are presented.

3.2 Energy Response and Resolution

The energy calibration was performed using a 450 MeV/c π^- beam scanning the 12 columns of the module. This is the higher available energy at the PSI beams and Monte Carlo simulations have shown that 450 MeV/c pions can be considered as minimum ionizing particles (*mips*) even after having traversed the complete thickness of the calorimeter module. The amount of energy that a minimum ionizing particles releases in an element of the module traversing it in the orthogonal direction, is called a *mip* and is the unit of energy. The comparison of the calibration at PSI with the calibration obtained with cosmic muons (see sect. 4) has shown no appreciable differences between the *mips* found, hence the 450 MeV/c π^- can be considered as *mips*.

Table 1 Energy response for electrons for different incidence angles

φ	θ	s_{em} $[mip/\mathrm{GeV}]$	offset $[mip]$
0^o	0^o	40.0 ± 0.2	-0.069 ± 0.028
20^o	0^o	39.0 ± 1.1	-0.019 ± 0.186
0^o	20^o	40.2 ± 0.8	-0.141 ± 0.104
0^o	40^o	40.0 ± 0.2	-0.195 ± 0.106

The measured energy (that is the calibrated sum over all the channels of both sides) as a function of the nominal energy of the beam is plotted in fig. 3 for different incidence angles. The superimposed straight line is a linear fit for the data at $\varphi = 0^o$ and $\theta = 0^o$. In table 1 the slopes s_{em} in mip/GeV and the offsets found for each angle configuration are given, showing that the offsets are compatible with 0 and that no dependence on the incidence angle is found for the slope. With a value of 3.24 MeV per *mip* from Monte Carlo simulations we obtain the sampling fraction for electromagnetic showers of $(13.0 \pm 0.1)\%$. In fig. 4 the ratio between the sigma σ_E and the mean $< E >$ values of the Gaussian energy distributions versus the nominal energy of the electrons is shown. The result is:

$$\frac{\sigma_E}{< E >} = \frac{(4.96 \pm 0.05)\%}{\sqrt{E(GeV)}}$$

with no contribution of an energy independent term. Values for non–zero incidence angles can be found in table 2, they agree very well with the one found for 0^o.

Table 2 Angular dependence of the energy resolution

φ	θ	$\sigma_E / < E > \times \sqrt{E}$ [%]
0^o	0^o	4.96 ± 0.05
20^o	0^o	5.08 ± 0.08
0^o	20^o	4.99 ± 0.06
0^o	40^o	4.96 ± 0.08

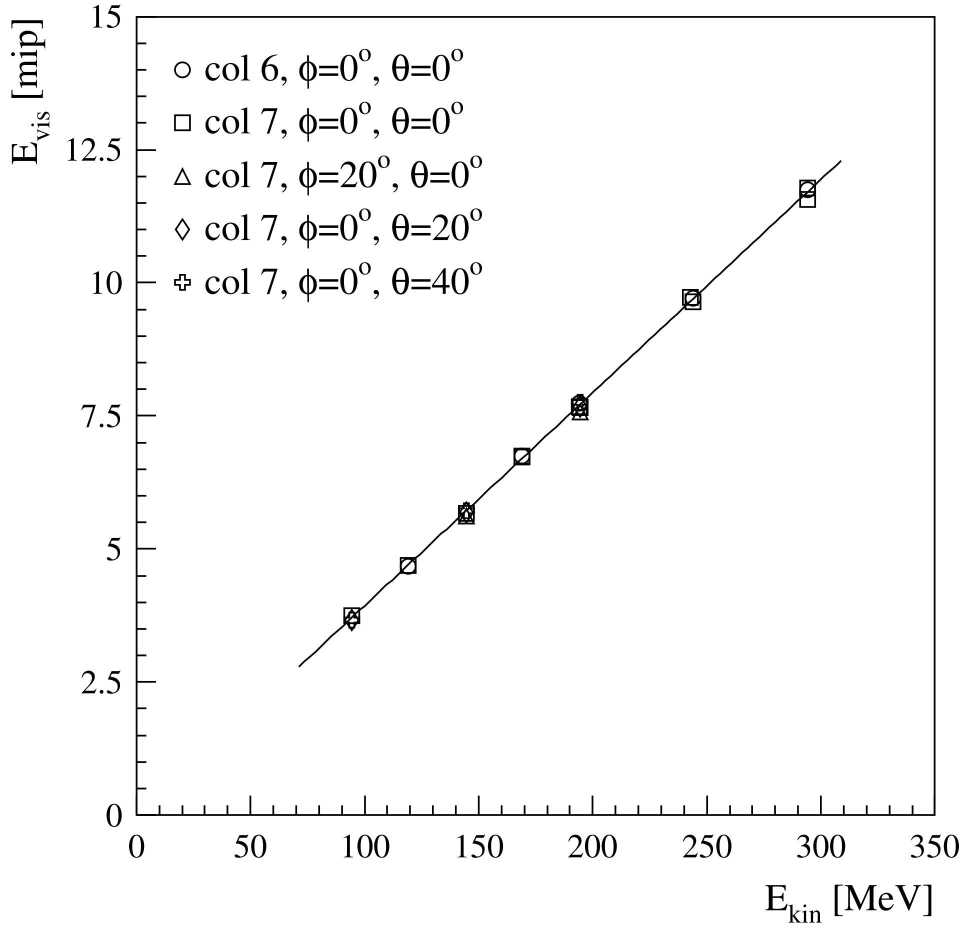

Fig. 3 Energy response for electrons, fit is for normal incidence only. Data are shown for two y impact positions, namely column 6 and 7, and for 4 angle configurations.

A weak dependence of the energy resolution on the position of the beam along the z-axis longitudinal to the fibers (the resolution at the module edge turns out to be about 5 % better than at the centre), has also been observed due to the contribution from the photoelectron statistics that depends on z for the attenuation of the light when travelling in the fiber.

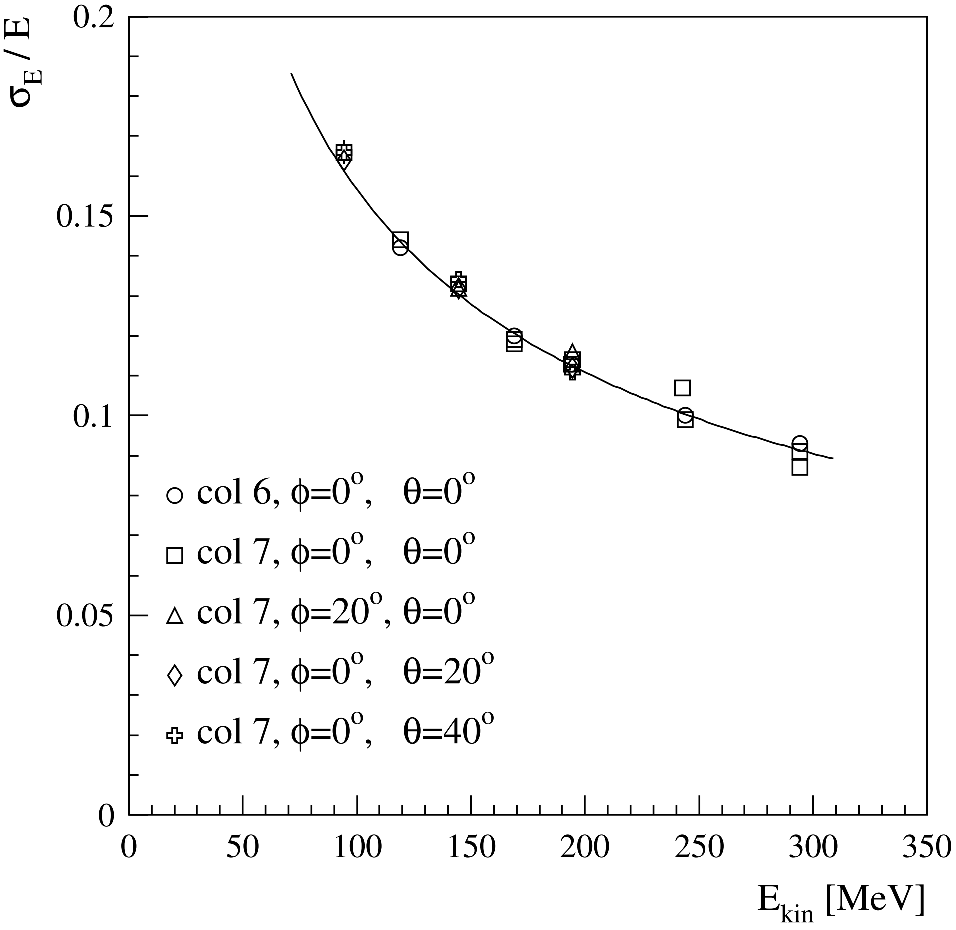

Fig. 4 Energy resolution for electrons as a function of the energy E_{kin}; fit is for normal incidence only.

3.3 Time Resolution

In order to express the event time the energy averaged sum over the individual times of the n hit elements

$$T_{sum} = \frac{1}{2} \sum_{i=1}^{n} \frac{(T_{A,i} + T_{B,i})(E_{A,i} + E_{B,i})}{(E_{A,i} + E_{B,i})}$$

is used. $E_{A,B}$ and $T_{A,B}$ are the energies and times on sides A and B respectively. To get the time resolution we fit the distribution of T_{sum} with a Gaussian and take its sigma value σ'_{Tsum}. This value still contains the jitter of the start σ_{start} which has to be subtracted quadratically to get the real time resolution σ_{Tsum}. A typical value for the time reference jitter was $\sigma_{start} = 180$ ps.

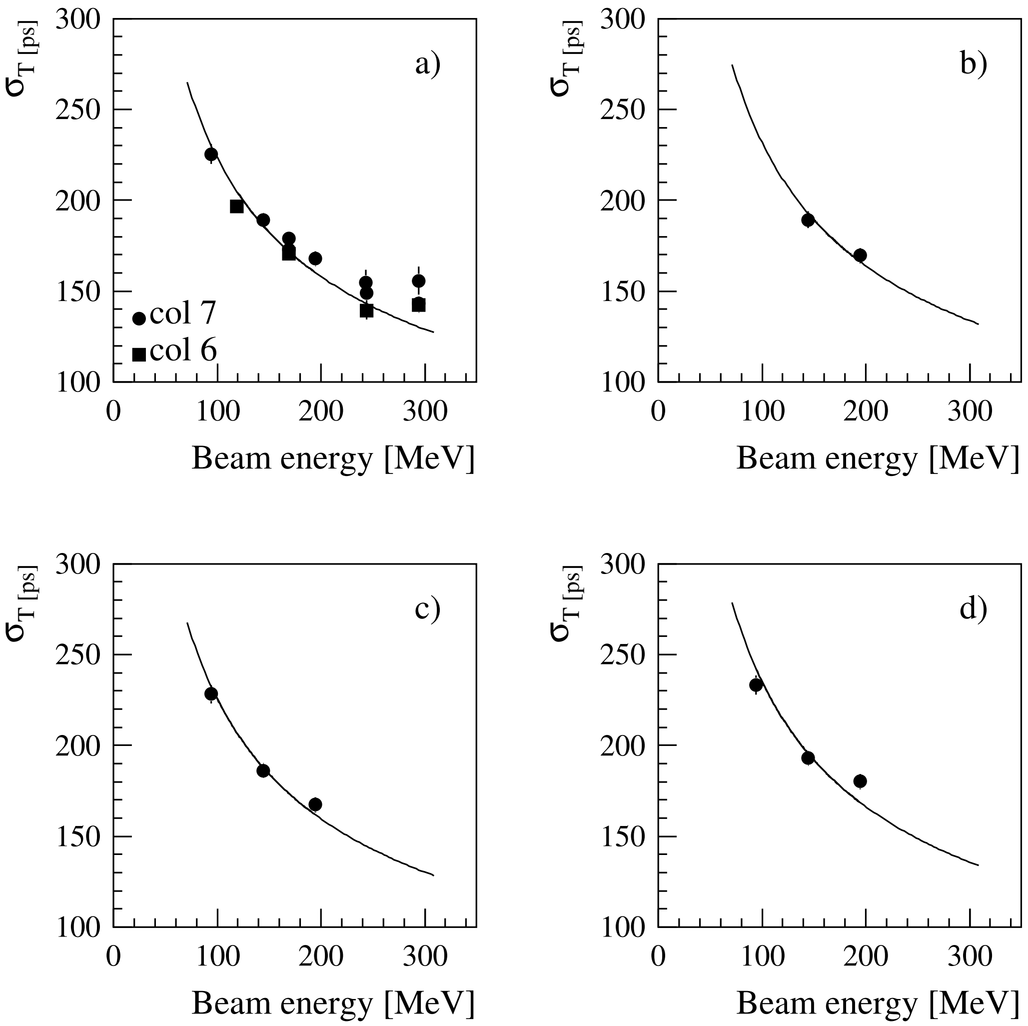

Fig. 5 Time resolution for electrons: a) $\varphi = 0^o$, $\theta = 0^o$, b) $\varphi = 20^o$, $\theta = 0^o$, c) $\varphi = 0^o$, $\theta = 20^o$, d) $\varphi = 20^o$, $\theta = 40^o$. In case a) data are shown at two impact positions, column 6 and 7.

In fig. 5 the time resolution is plotted vs. the nominal energy for electrons at various incidence angles. The curves can be described by a $1/\sqrt{E}$ dependence. For 0^o incidence angles we get

$$\sigma_{Tsum}(E) = \frac{(72 \pm 1)\text{ps}}{\sqrt{E(GeV)}}$$

For non–zero values of the incidence angles we get the slightly worse values that are listed in table 3.

Table 3 Angular dependence of the time resolution

φ	θ	$\sigma_T \times \sqrt{E}$ ps
0^o	0^o	71.7 ± 1.0
20^o	0^o	73.3 ± 1.3
0^o	20^o	71.4 ± 0.9
0^o	40^o	74.4 ± 1.0

The time resolution is dominated by photoelectron statistics hence a larger effect for the time resolution than for the energy resolution when moving from the centre of the module towards the edges is observed. The time resolution at the edges is about 15 % worse than at the centre.

Finally from the time difference between the two PM's looking at the same element we get the z–coordinate. The spatial resolution in the z–direction σ_z after subtraction of the beam spot extension, is shown in fig. 6 as a function of the energy for electrons at normal incidence. A fit gives the following energy dependence:

$$\sigma_z(E) = \frac{(1.2 \pm 0.1)\text{cm}}{\sqrt{E(GeV)}}$$

3.4 Comparison with prototype results

When we compare these results with the energy and time response obtained from the smaller size 2 m long prototype[2] we find a slightly increased energy resolution (from 4.5 to 5.0 $\%/\sqrt{E}$) and a nearly doubled time resolution (from 35 to 70 ps$/\sqrt{E}$). Both results can be explained in term of loss of photoelectrons due mainly to the use of smaller quantum efficiency PM's (of the order of 60 % with respect to the quantum efficiency of standard PM's like those used in the prototype test) and to the increased length of the module itself. The loss of photoelectrons affects directly the time resolution (that has a $1/\sqrt{N_{pe}}$ behaviour) and the photon statistics contribution to the energy resolution (that is of the order of $2.5\%/\sqrt{E(GeV)}$ as discussed in ref. 2).

Better time resolution is expected both by using an improved version of fine mesh PM's[5] and also improved fibers in the rear second half of the calorimeter[6]. We estimate a time resolution of 50 ps$/\sqrt{E(GeV)}$ and an energy resolution of $4.7\%/\sqrt{E(GeV)}$ for the final version of the calorimeter.

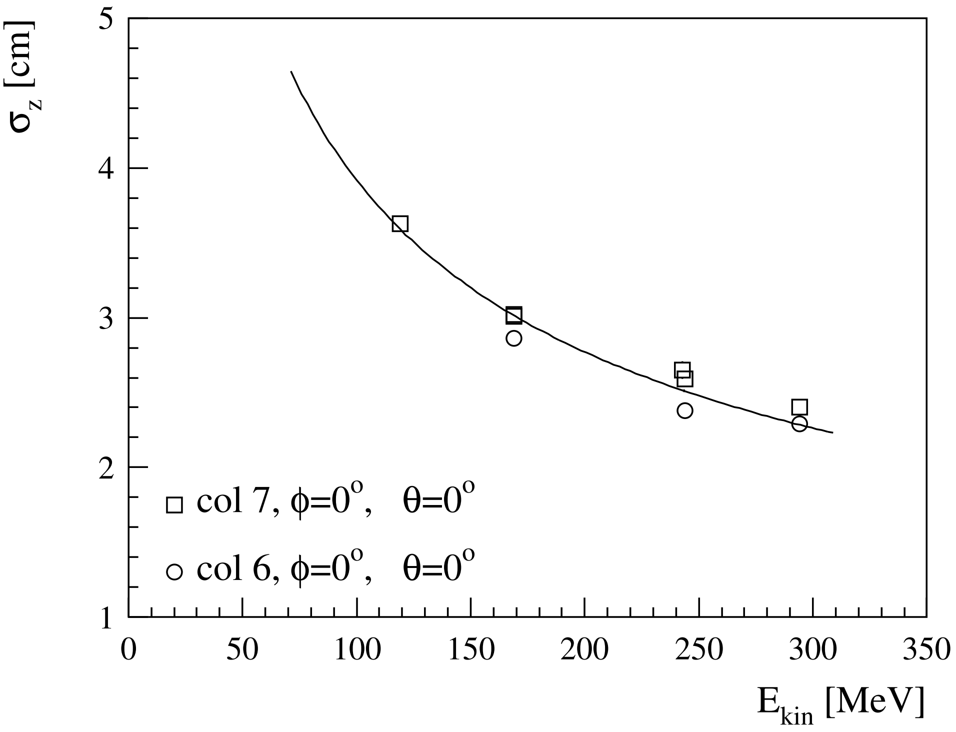

Fig. 6 z–resolution vs. kinetic energy for electrons at normal incidence.

4. Results from continuous monitoring with cosmic rays

In the second half of 1994 the production of the 24 modules of the barrel part of the KLOE electromagnetic calorimeter has began. In order to provide a simple method for testing the modules, a Cosmic Ray Test Stand has been built at the Frascati Laboratories. This facility consists of a cosmic ray telescope made of scintillation counters and limited streamer tubes providing a tracking of cosmic minimum ionizing particles (*mip*s). Testing a module in this stand will allow us to obtain:

(1) a simple measurement of the main calibration parameters (*mip*s, attenuation lengths, light velocities and $\Delta T_0'$s) for each element of the module;

(2) a long term monitoring of these parameters in order to check the stability of the overall device, including the detector and the front end electronics.

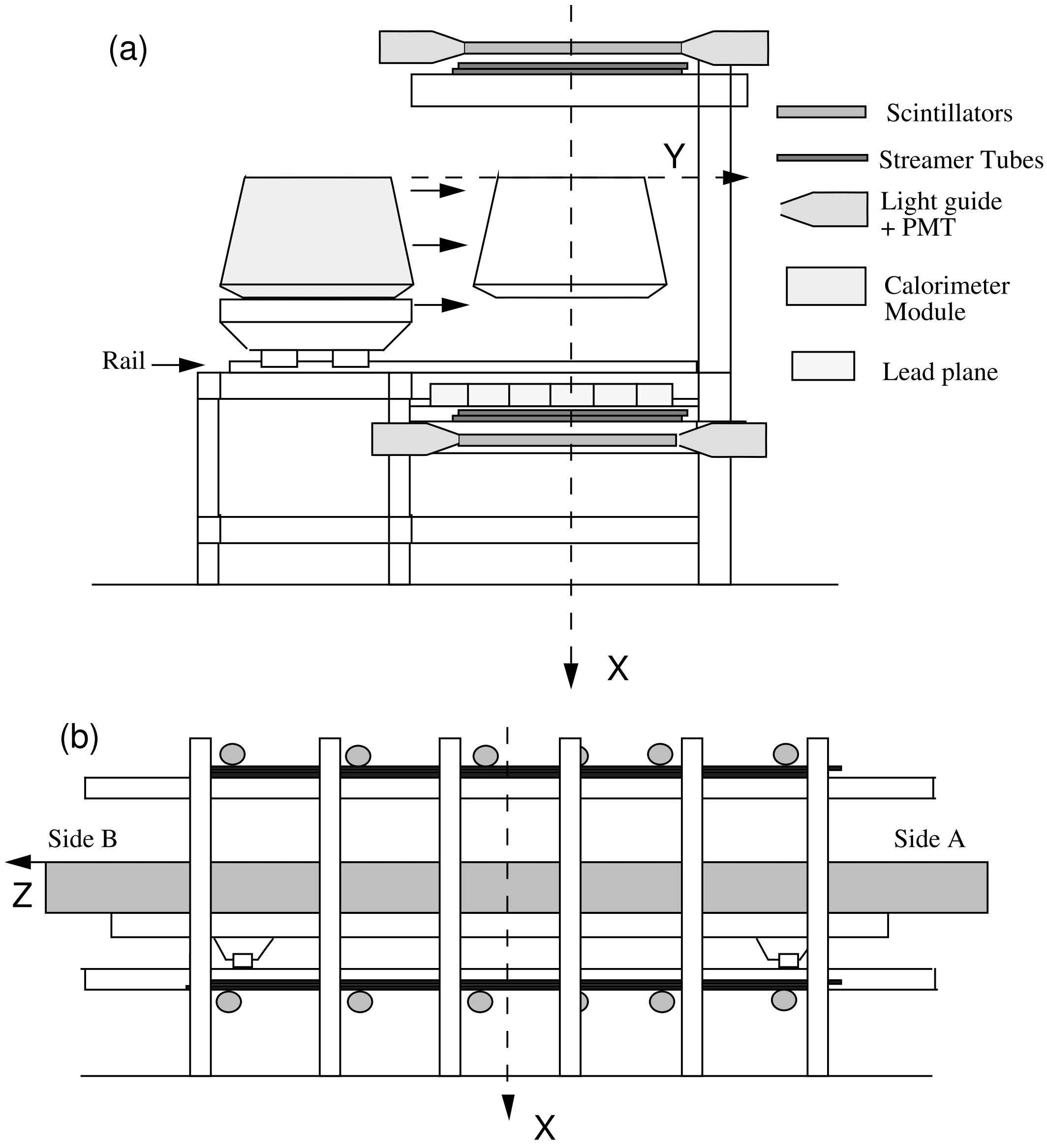

Fig. 7 Sketch of the set-up of the cosmic ray test stand. (a) Front view and (b) side view. Not in scale.

4.1 Experimental Set-up

A sketch of the set-up is shown in fig. 7. The calorimeter module under test, is positioned on a platform that can be inserted and removed through two rails, in the 60 cm wide space between the top and bottom halves of the telescope. A mechanical structure supports both the platform and the two halves of the telescope.

Each half of the telescope consists of:

(i) six 60×7 cm^2 NE110 scintillator slabs 2 cm thick viewed at both ends by EMI

9814B photomultipliers;

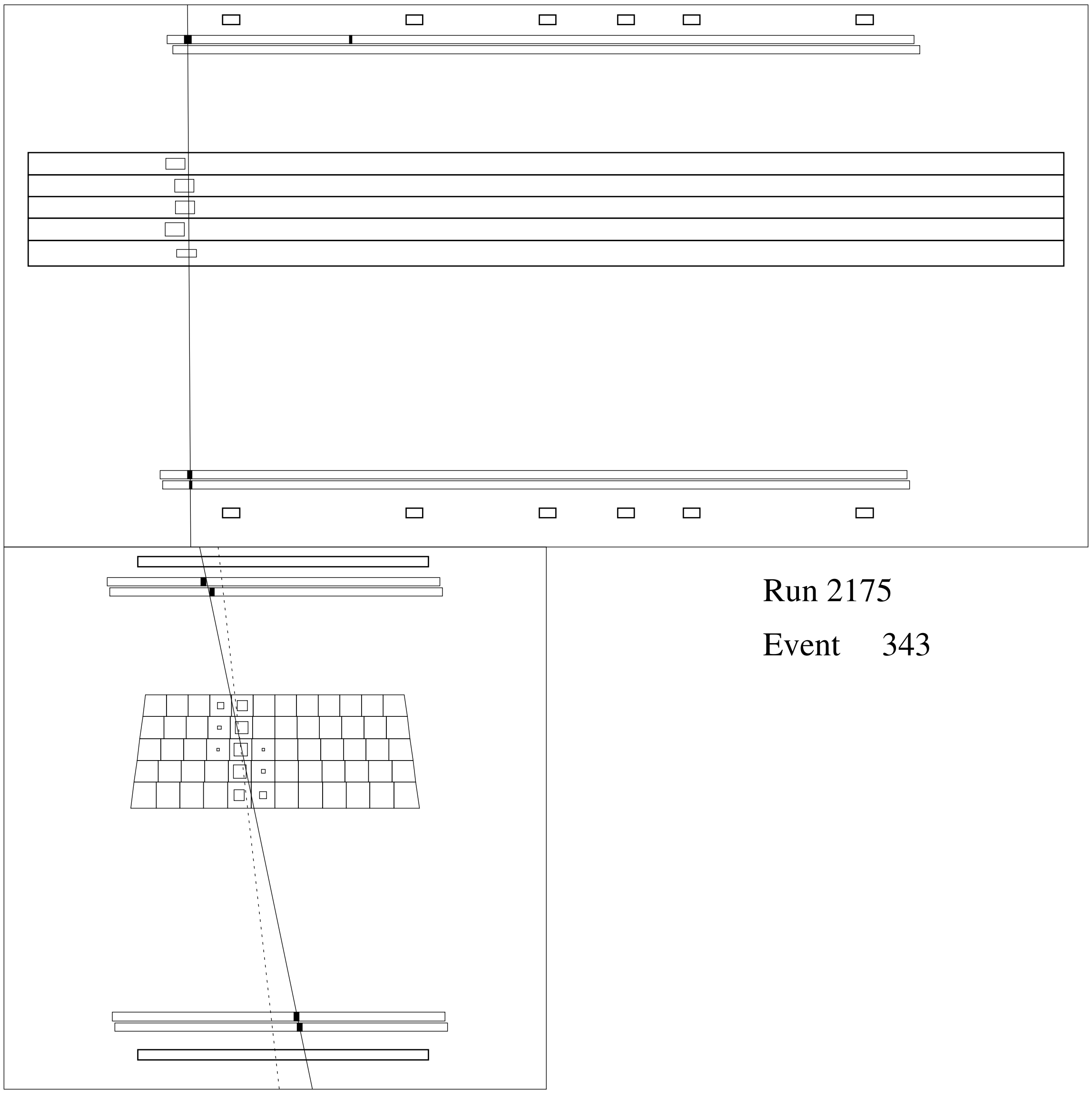

Fig. 8 Example of a cosmic ray event as given by the on-line Event Display. The solid line is the track obtained by fitting the LST hits. Every module channel is shown by a rectangle proportional to the ADC content in the x-y view and by a rectangle in the position reconstructed by the time difference in the x-z view.

(ii) 2 layers of superimposed 310×64 cm^2 planes of Limited Streamer Tubes (LST) operated with a standard Argon-Isobutane mixture (30%-Ar 70%-Isobut.) at 4450 V. Both longitudinal and transverse read-out are provided by 1 cm pitch aluminum strips while the signals from the wires are used for the trigger system.

Furthermore a 5 cm thick lead layer is inserted between the module and the bottom half of the telescope to harden the energy spectrum of the particles that trigger the system.

For triggering we use: a scintillator based trigger requiring at least one counter in the top half and one in the bottom half and a LST based trigger requiring at least one hit in the top half and one in the bottom half. The LST trigger has a higher rate ($30 \div 40$ Hz against $2 \div 3$ Hz of the scintillator trigger) due to the wider surface and angular coverage with respect to the scintillators. On the other hand the scintillator trigger provides a better time reference for timing studies, the LST trigger being affected by a much larger time jitter.

Fig. 8 shows an example of cosmic ray event as given by the on-line event display.

4.2 *mip*S AND ATTENUATION LENGTHS MEASUREMENT

The value of the *mip* signal and of the attenuation length for every module element is measured as follows. Tracks are selected that have an angle respect to the vertical direction less than 15^o and that intersect the element in the y coordinate; then the dependence of the pulse height on the z impact position of the track on the element is obtained for both sides A and B of every element (see Fig. 9 as an example). An exponential fit gives (i) the attenuation length and (ii) the value of the pulse height (in ADC counts) at $z = 0$ (that is the *mip*).

The accuracy in the evaluation of λ and of the *mip* depends on the amount of collected statistics: uncertainties in the range $5 \div 10$ cm on λ and $0.3 \div 0.5$ *ADC* counts on the *mip* are obtained in 4 days of run.

Fig. 10 shows the measured values of attenuation length and of mip averaged over all the elements of the same plane, as a function of the plane number. The first two planes correspond to the part of the module equipped with Kuraray fibers, the third plane corresponds to 50% Kurary and 50% Pol.Hi.Tech. fibers and the two last planes correspond to only Po.Hi.Tech. fibers. We notice here that the Pol.Hi.Tech. used for the Module 0 were delivered in 1994, the 1995 production being of rather better quality[6] . The comparison between Kuraray and Pol.Hi.Tech. is in agreement with previous independent tests on these fibers[3] .

We have looked also for possible long term variations of these parameters, in the period from July 1994 (test on beam at PSI) up to June 1995. In this context we have verified that the λ's are stable within our accuracy whilst we have observed uncorrelated *mip*s variations up to $\pm 10\%$ which is much higher than our measurement uncertainty. These variations have a mean value compatible with 0 and are mostly attributed to possible long term gain drifts of the PM's.

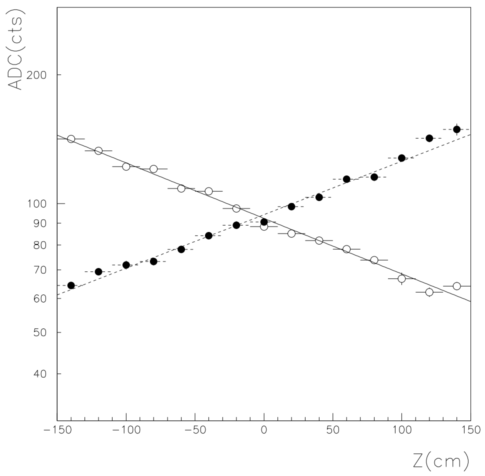

Fig. 9 Dependence of the ADC response on the z impact position of the cosmic track for the side A (open circles) and side B (full circles) of one element.

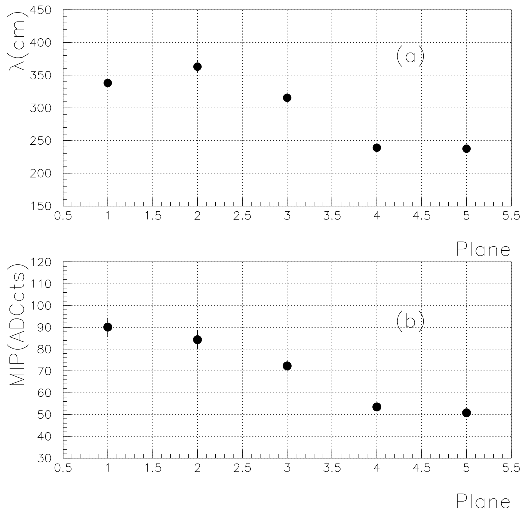

Fig. 10 (a) Average attenuation length as a function of the plane number. (b) Average *mip* value as a function of the plane number. Planes 1 and 2 are equipped with Kuraray SCSF-81 fibers, planes 4 and 5 with Pol.Hi.Tech. 00046 fibers. Plane 3 has 50% Kuraray and 50% Pol.Hi.Tech..

4.3 Light velocities and ΔT_0 measurement

In this section preliminary results concerning the ΔT vs z relation are presented.

The dependence of the time difference ΔT between the two sides of an element on the z impact position of the track along the fiber direction is shown in fig. 11 for one element. A linear fit on this dependence gives a slope that is half of the light velocity within the fibers, and an offset that is the difference between the T_0's of the two sides. Since in the difference the jitter on the time reference is cancelled out, the LST triggers can also be used in this analysis.

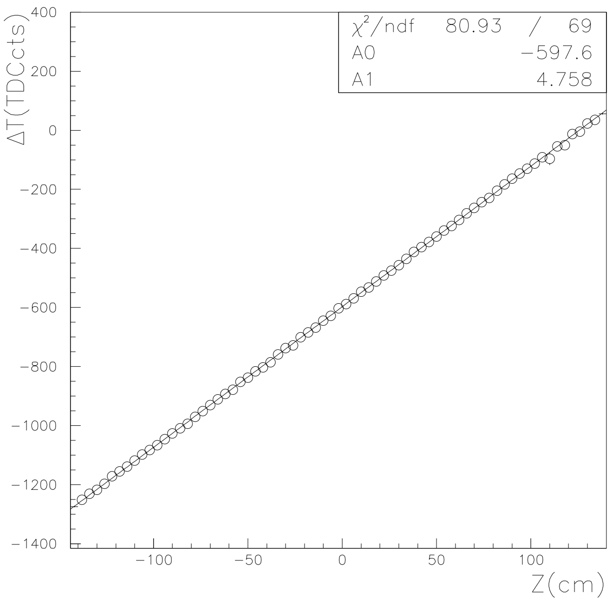

Fig. 11 Time difference ΔT as a function of the z of the impact position of the track. The linear fit giving the average light velocity along the fibers is superimposed.

From the fit, the light velocity is obtained with a statistical uncertainty of $0.2 \div 0.3\%$, and the $\Delta T_0'$ with an uncertainty of about 10 ps. A systematical uncertainty on the light velocity measurement of the order of 1.5% is observed due to possible miscalibration between the different TDC channels (with a nominal 25 ps/channel calibration). If we correct the value coming from every TDC channel using relative calibration constants obtained by special intercalibration measurements with computer driven pulses, the spread of the light velocities is reduced from 1.5% to about 0.3 % that is in agreement with the statistical uncertainty of the measurement. The value of the light velocity in the fibers obtained by averaging over all the elements and using the nominal value of 25 ps/channel for the TDC calibration is 16.9 cm/ns $\pm$ 0.05($stat$) $\pm$ 0.25($syst$), the large systematical uncertainty being due mainly to the TDC absolute calibration.

No long term variations in excess of the measurement uncertainty are observed for the light velocities, while variations are observed for ΔT_0 of the order of more than $40 \div 50$ ps. Such variations are interpreted as due to electronic effects or to cable length variations.

ACKNOWLEDGEMENTS

We wish to express our gratitude to M. Anelli and M. Bertino for their skilful work in the set-up of the test beam and of the cosmic ray test stand. We acknowledge also F. Basti, C. Piscitelli and G. Rossi for their technical support.

REFERENCES

1. The KLOE Detector Technical Proposal, the KLOE Collaboration, LNF-92/019 (IR), Jan. 21 1993;
2. A. Antonelli et al., Nucl.Instr. and Meth. **A354** (1995) 352;
3. A. Antonelli et al., submitted to Nucl.Instr. and Meth.;
4. A. Antonelli et al., submitted to Nucl.Instr. and Meth.;
5. Hamamatsu Photonics is producing an improved version of 1.5 in. mesh PM's with a quantum efficiency at the level of standard linear focussed PM's, so about a factor of two better than the PM's used in the tests described here.
6. The latest Pol.Hi.Tech. 0046 fibres have an attenuation length and a light yield comparable with that of Kuraray SCSF-81.